PROTOPLANETARY DISKS INCLUDING RADIATIVE FEEDBACK FROM ACCRETING PLANETS

MATÍAS MONTESINOS[1,2,3], JORGE CUADRA[2], SEBASTIAN PEREZ[1,3], CLÉMENT BARUTEAU[4], AND SIMON CASASSUS[1,3]

[1] Departamento de Astronomía, Universidad de Chile, Casilla 36-D, Santiago, Chile; montesinos@das.uchile.cl, sperez@das.uchile.cl, scasassus@das.uchile.cl
[2] Instituto de Astrofísica, Pontificia Universidad Católica de Chile, Santiago, Chile; jcuadra@astro.puc.cl
[3] Millennium Nucleus "Protoplanetary Disks", Chile
[4] Institut de Recherche en Astrophysique et Planétologie, CNRS/Université de Toulouse/UPS-OMP, 14 avenue Edouard Belin, F-31400 Toulouse, France; Clement.Baruteau@irap.omp.eu

ABSTRACT

While recent observational progress is converging on the detection of compact regions of thermal emission due to embedded protoplanets, further theoretical predictions are needed to understand the response of a protoplanetary disk to the radiative feedback from planet formation. This is particularly important to make predictions for the observability of circumplanetary regions. In this work we use 2D hydrodynamical simulations to examine the evolution of a viscous protoplanetary disk in which a luminous Jupiter-mass planet is embedded. We use an energy equation that includes the radiative heating of the planet as an additional mechanism for planet formation feedback. Several models are computed for planet luminosities ranging from 10^{-5} to 10^{-3} solar luminosities. We find that the planet radiative feedback enhances the disk's accretion rate at the planet's orbital radius, producing a hotter and more luminous environement around the planet, independently of the prescription used to model the disk's turbulent viscosity. We also estimate the thermal signature of the planet feedback for our range of planet luminosities, finding that the emitted spectrum of a purely active disk, without passive heating, is appreciably modified in the infrared. We simulate the protoplanetary disk around HD 100546 where a planet companion is located at about 68 AU from the star. Assuming the planet mass is five Jupiter masses and its luminosity is $\sim 2.5 \times 10^{-4} L_\odot$, we find that the radiative feedback of the planet increases the luminosity of its ~ 5 AU circumplanetary disk from $10^{-5} L_\odot$ (without feedback) to $10^{-3} L_\odot$, corresponding to an emission of ~ 1 mJy in the L' band after radiative transfer calculations, a value that is in good agreement with HD 100546b observations.

Key words: accretion, accretion disks – hydrodynamics – methods: numerical – planet–disk interactions – planetary systems – protoplanetary disks

1. INTRODUCTION

Recent observational progress allows the detailed study of planet formation feedback. The ALMA facility has opened the resolved study of accretion kinematics in protoplanetary gaps. For instance, Casassus et al. (2012, 2013) find that the dust gap in the disk around the star HD 142527 shows a disrupted outer disk suggestive of on-going dynamical clearing, and contains residual gas whose kinematics are consistent with accretion across the dust gap. Dramatic advances in high-contrast imaging techniques have allowed the likely detection of embedded protoplanets. Quanz et al. (2013a) found a compact but resolved 3.8 μm (L') source at ~ 68 AU from HD 100546 (independently confirmed by Currie et al. 2014), which could be interpreted as on-going accretion onto a compact body. In another example of resolved data, Quanz et al. (2013b) present polarized light images of HD 169142 resolving features in its protoplanetary disk that could be interpreted as a gap induced by forming protoplanets. Indeed, Reggiani et al. (2014) and Biller et al. (2014) find an L' point source, within this gap, at a separation of ~ 22 AU. There are indications that this L' compact signal is not photospheric, and that it is somehow connected to the protoplanetary accretion luminosity. Similar findings have been reported for the compact Hα signal found at 12 AU from HD 142527 by Close et al. (2014), which coincides with a relatively bright L' signal. That source would reach the stellar mass regime for photospheric emission (Biller et al. 2012), but has been recently resolved to be extended and polarized in the Y band (Rodigas et al. 2014), suggesting that this companion to HD 142527 is probably a substellar object with a remarkably strong thermal luminosity in L', that is somehow connected to accretion.

Hydrodynamical simulations can be used to study the dynamical effects of accretion feedback (e.g., Nayakshin & Cha 2013), and to inform the interpretation of the data on planet-forming systems, by calculating the radiative emissions of a disk with an embedded planet that has created a gap. This was the approach used by Wolf & D'Angelo (2005), who modeled in two dimensions the gravitational response of a disk to the presence of an embedded planet, under the assumption of a constant aspect ratio for the disk. As a post-processing step, once the simulation reached steady state, Wolf and D'Angelo assumed a luminosity for the planet and calculated the radiative response of the disk. They concluded that a hot circumplanetary region could eventually be detected by ALMA.

In this paper we also use 2D hydrodynamical simulations to follow the dynamics of a disk with an embedded planet. However, instead of assuming a temperature profile for the disk, we use a non-stationary energy equation that includes the radiative feedback of planet formation and a temperature-dependent blackbody cooling for the disk.

The structure of the paper is as follows: in Section 2 we present the model including the main assumptions, the physical conditions of the disk, as well as the numerical set-up and a description of the code. Our results and main conclusions of the evolution of the density profile, temperature, and the spectral signature of the disk are presented in Section 3, with a short discussion in Section 4. We summarize our findings in Section 5.

2. THE MODEL

We are interested in the evolution of a gaseous proto-planetary disk in which a luminous Jupiter-mass planet is embedded. In our simulations we use an energy equation that includes radiative cooling, and both viscous heating and heating due to the planet's luminosity. We follow the evolution of the protoplanetary disk for about 10^4 years, assuming the planet is already formed at the beginning of the simulations. This is a short period of time compared with both the lifetime of protoplanetary disks ($\sim$Myr e.g., Williams & Cieza 2011), and the timescales over which planet luminosities should vary (Marley et al. 2007; Mordasini 2013), thus justifying the use of a constant planet luminosity in the simulations.

Our simulations use the public two-dimensional hydrody-namics code FARGO-AD[5] (Baruteau & Masset 2008) which is dedicated to planet–disk interactions. It is a staggered mesh code that solves the Navier–Stokes, continuity, and energy equations on a polar grid. It is based on an Eulerian formalism using a finite difference method of second order, according to the van Leer (1977) upwind algorithm. Details of the code can be found in Masset (2000) and Baruteau & Masset (2008). In FARGO-AD's public version, the energy equation includes viscous heating and a simple temperature relaxation to reach thermodynamical equilibrium over some (user-defined) char-acteristic timescale.

The present work features two main changes to the energy equation. One is the inclusion of a radiative cooling function, based on the assumption that the disk radiates locally as a blackbody. The second, and most important feature, is the implementation of a heating source term associated to the planet. We assume that the protoplanet has an intrinsic constant luminosity; therefore, it injects energy into the disk at a constant rate. We only take into account the gravitational potentials of the star and of the planet; the disk's self-gravity is neglected.

2.1. Code Units and Initial Setup

We set the mass of the central star ($M_\star$) and the planet's orbital radius (r_p) as the code's units of mass and length, respectively. The code's unit of time (t_0) is the planet's orbital period divided by 2π, that is $t_0 = (GM_\star/r_p^3)^{-1/2}$. The gravitational constant $G = 1$ in code units. The code's unit of temperature is $GM_\star \mu m_p/(k_B r_p)$, with μ the mean molecular weight of the gas ($\mu = 2.35$ in all our simulations), m_p the proton mass, and k_B the Boltzmann constant. Unless otherwise noted (see Section 3.6), we adopt a solar-mass star ($M_\star = M_\odot$) and a planet at $r_p = 10$ AU.

We use cylindrical coordinates (r, ϕ). The computational domain extends from $r = 1$ to 50 AU over $n_r = 400$ equally spaced radial rings. It covers the full 2π extent in azimuth over $n_\phi = 800$ equally spaced azimuthal sectors. Tests with higher grid resolutions, $n_r \times n_\phi = 512 \times 1536$, were performed to check the convergence of our results. We use open inner and outer boundary conditions, meaning that the material is allowed to outflow at the disk edges.

The initial density profile scales with r^{-1}:

$$\Sigma(r) = \Sigma_0 \frac{r_p}{r}, \qquad (1)$$

where $\Sigma_0 = 2.56 \times 10^{-5} M_\odot$ AU^{-2}. This initial disk mass is thus $10^{-3} M_\odot$. The disk's aspect ratio $h = c_s/v_K$, with c_s the isothermal sound speed and v_K the Keplerian velocity, initially equals 0.05, uniformly. The disk's initial temperature therefore decreases in r^{-1} and is $\approx$63 K at 10 AU for our fiducial primary mass ($M_\star = M_\odot$).

We fix the planet-to-primary mass ratio (q) to $q = 10^{-3}$, so the planet has a Jovian mass for a solar-mass star. The planet is held on a fixed circular orbit (it does not migrate through the disk). To avoid a violent response of the disk to the planet's gravitational potential initially, the planet mass is increased gradually over the first five orbits according to

$$M(t) = M_p \sin^2\left(\pi t/10 T_p\right), \qquad (2)$$

where T_p is the planet's orbital period. We adopt three values for the planet's luminosity: 10^{-5}, 10^{-4}, and 10^{-3} $L_\odot$ (see Section 2.3.2). For the viscosity prescription, in our fiducial model we use an alpha disk model (Shakura & Sunyaev 1973), setting $\alpha = 4 \times 10^{-3}$ (but see Section 3.4).

2.2. The Energy Equation

The energy equation satisfied by the thermal energy density e reads (e.g., D'Angelo et al. 2003)

$$\frac{\partial e}{\partial t} + \boldsymbol{\nabla} \cdot (e\boldsymbol{v}) = -P\boldsymbol{\nabla} \cdot \boldsymbol{v} + Q^+ - Q^-, \qquad (3)$$

where $\boldsymbol{v}$ is the gas velocity, P the pressure, Q^+ the heating rate per unit area, and Q^- the radiative cooling rate per unit area. To close the system of equations, an ideal equation of state is used,

$$P = \Sigma T \overline{R}, \qquad (4)$$

with T the gas temperature and $\overline{R} = k_B/\mu m_p$. The thermal energy density is related to the temperature through

$$e = \Sigma T \left(\frac{\overline{R}}{\gamma - 1}\right), \qquad (5)$$

where γ denotes the adiabatic index, which we fix to $\gamma = 1.4$ (a typical value for a diatomic gas). Equation (3) can be recast as

$$\frac{\partial e}{\partial t} + \boldsymbol{\nabla} \cdot (e\boldsymbol{v}) = -(\gamma - 1)e\boldsymbol{\nabla} \cdot \boldsymbol{v}$$
$$+ Q_v^+ + Q_p^+ - Q^-, \qquad (6)$$

where Q_v^+ is the viscous heating rate, Q_p^+ the flux of radiative energy received from the planet (feedback), and Q^- corre-sponds to the radiative cooling rate of the disk. These source terms are detailed in the next section.

In a more realistic situation, a thermal diffusion flux term should be added on the right side of Equation (6). But, since the outer temperature of the circumplanetary disk (CPD) matches that of the protoplanetary disk, we expect no strong heat diffusion to occur.

2.3. Sources of Heating and Cooling

2.3.1. Viscous Dissipation

The viscous heating rate implemented in FARGO-AD, Q_v^+, has two contributions. The first one arises from the shear

---

kinematic viscosity ν,

$$Q_{\text{shear}}^{+} = \frac{1}{2\nu\Sigma}\left[\tau_{r,r}^2 + 2\tau_{r,\phi}^2 + \tau_{\phi,\phi}^2\right] + \frac{2\nu\Sigma}{9}(\boldsymbol{\nabla}\cdot\boldsymbol{v})^2, \quad (7)$$

where the $\tau_{\alpha,\beta}$ are the components of the viscous stress tensor:

$$\tau_{r,r} = 2\nu\Sigma\left[\frac{\partial v_r}{\partial r} - \frac{1}{3}\boldsymbol{\nabla}\cdot\boldsymbol{v}\right],$$

$$\tau_{r,\phi} = \nu\Sigma\left[r\frac{\partial}{\partial r}\left(\frac{v_\phi}{r}\right) + \frac{1}{r}\frac{\partial v_r}{\partial \phi}\right],$$

$$\tau_{\phi,\phi} = 2\nu\Sigma\left[\frac{1}{r}\frac{\partial v_\phi}{\partial \phi} + \frac{v_r}{r} - \frac{1}{3}\boldsymbol{\nabla}\cdot\boldsymbol{v}\right]. \quad (8)$$

Note that for a Keplerian disk (i.e., $v_r = 0$, $v_\phi = r\Omega_K$ with Ω_K the Keplerian angular frequency), $\tau_{r,r} = \tau_{\phi,\phi} = 0$ and the shear viscous heating rate reduces to $Q_v^+ = \tau_{r,\phi}^2/\nu\Sigma = \frac{9}{4}\nu\Sigma\Omega_K^2$.

The second contribution to the viscous heating rate is through the use of a von Neumann–Richtmyer artificial bulk viscosity, as described in Stone & Norman (1992), where the coefficient C_2 is taken equal to 1.4 (C_2 measures the number of zones over which a shock is spread over by the artificial viscosity).

2.3.2. Planet Feedback

The key feature in this work is the inclusion of the planet feedback (i.e., the energy flux received from the protoplanet by the gas disk) during its evolution. In this initial study, we use a simplified model for the planet luminosity, which is powered by its mass build-up during its formation and evolution. Assuming free-fall, the typical power dissipated during the formation of a Jupiter-like planet is

$$\dot{E}_J = \frac{GM_J^2}{R_J t_p}, \quad (9)$$

where M_J and R_J are the mass and radius of Jupiter, respectively, and t_p is a characteristic timescale for its formation.

A characteristic timescale obtained from ground-based and *Spitzer*-based infrared (IR) surveys of young stellar clusters, which trace the evolution of primordial protoplanetary disks, suggest a formation period of about ∼3×10^6 years (Mamajek 2009). Then, the emitted energy (Equation (9)) reads $\dot{E}_J \simeq 1 \times 10^{-4}\ L_\odot$, which also agrees with hot accretion shock structure formation models (e.g., Mordasini 2013). To account for the large uncertainties in the accretion process of planetesimals, we adopt planet luminosities L_p ranging from $10^{-1}\dot{E}_J$ to $10\dot{E}_J$ (i.e., 10^{-5}–$10^{-3}\ L_\odot$).

In our model, the planet has already reached its final mass at the beginning of the simulation, and no longer grows. In that sense the origin of the planet luminosity should be thought as a post-formation luminosity during the slow contraction of the planet rather than accretion luminosity, However, it is still possible that with opacities larger than those commonly used (e.g., Bell & Lin 1994) the accretion shock luminosity takes much more time to be released, and therefore the total planet luminosity might include contributions of both aforementioned sources. Also, it should be noticed that the high luminosities we are using (i.e., $L_p = 10^{-3}\ L_\odot$) are expected for larger opacities under the assumption of a hot accretion formation model

(Mordasini 2013). On the other hand, *cold accretion* initial conditions produce much smaller (post-formation) planet luminosities ($\lesssim 10^{-4}\ L_\odot$), but current models of giant planet formation cannot distinguish between *cold* and *hot* start initial conditions; as such, one model cannot be preferred over the other. We assume a hot accretion initial planet formation model in this work, focusing on studying the effect of high planet luminosities.

In all our simulations, the planet's CPD is optically thick. The thermal energy released by the planet is therefore chosen to be distributed isotropically within the planet's CPD, the size of which is denoted by R_{CPD}. Following Crida et al. (2009), we adopt $R_{\text{CPD}} = 0.6R_{\text{Hill}}$, where $R_{\text{Hill}} = r_p(q/3)^{1/3}$ is the planet's Hill radius. To avoid possible thermal shocks at the beginning of the simulation, we gradually inject the planet energy in the same way as we do for the planet mass (see Equation (2)), i.e., following $Q_p^+(t) = Q_p^+ \sin^2(\pi t/10T_p)$, with T_p the planet's orbital period, and

$$Q_p^+ = \begin{cases} f(r)L_p/\left(\pi R_{\text{CPD}}^2\right) & \text{if } r = |\boldsymbol{r} - \boldsymbol{r}_p| < R_{\text{CPD}} \\ 0 & \text{otherwise,} \end{cases} \quad (10)$$

where $f(r)$ is a Gaussian function used to smoothly inject the planet energy within the CPD. Its expression is $f(r) = A\exp(-5d^2/R_{\text{CPD}}^2)$, where A is a dimensionless normalization factor equal to 5. It has a FWHM of ∼$0.75R_{\text{CPD}}$.

It is worth noting that our model shows some inherent limitations due to the 2D geometry. For instance, we are assuming that the injected energy from the planet is only transported through the r–ϕ plane of the CPD, missing the radiation escaping in the vertical direction. This could lead to an overestimate of the thermal energy deposited in the disk.

2.3.3. Radiative Cooling and Disk Spectrum

The cooling term Q^- in Equation (6) corresponds to the energy flux radiated by the disk in the vertical direction. This quantity depends on whether the disk is optically thin or thick. Several processes could be responsible for the energy evacuation, e.g., for high temperatures (∼10^4 K) Thomson scattering processes, free–free, and bound–free transitions are dominant. For lower temperatures, e.g., ∼1–10^3 K, as in our case, Rosseland and Planck mean opacities of dust and grain species should be used (e.g., Bell & Lin 1994; Semenov et al. 2003).

In our models, we calculate the optical depth ($\tau = \kappa\Sigma/2$) assuming the Rosseland mean opacity κ from Bell & Lin (1994). In some regions of the disk, the gas density could be diluted (e.g., at the gap and/or planet's location), and become transparent or less opaque ($\tau \sim 1$). We use the Hubeny (1990) prescription to calculate the effective optical depth,

$$\tau_{\text{eff}} = \frac{3\tau}{8} + \frac{\sqrt{3}}{4} + \frac{1}{4\tau}. \quad (11)$$

The effective temperature (T_{eff}) and mid-plane temperature (T) are then related through

$$T_{\text{eff}}^4 = \frac{T^4}{\tau_{\text{eff}}}. \quad (12)$$

The cooling rate per unit area due to radiation from the surface of the disk is calculated by integrating the total emitted

radiative flux Φ_ν over all frequencies,

$$Q^-(r) = 2 \int_0^\infty \Phi_\nu\big(T_{\text{eff}}(r, \phi)\big)d\nu, \qquad (13)$$

where $\Phi_\nu(T_{\text{eff}}(r, \phi))$ is the local emergent flux of the disk surface. The factor of two is needed because radiation escapes from both sides (top and bottom) of the disk. For simplicity, we assume that the local emitted flux is given by the blackbody approximation,

$$\Phi_\nu(T) = 2\pi B_\nu\big(T_{\text{eff}}(r, \phi)\big), \qquad (14)$$

where $B_\nu(T_{\text{eff}}(r, \phi))$ is the Planck function and $T_{\text{eff}}(r, \phi)$ is the surface disk temperature.

The spectrum of the disk is calculated by integrating the emitted flux $\Phi_\nu(T_{\text{eff}}(r, \phi))$ (Equation (14)) over the surface of the disk,

$$L_\nu = \int \Phi_\nu\big(T_{\text{eff}}(r, \phi)\big)r dr d\phi. \qquad (15)$$

Using Equation (15) we calculate the bolometric luminosity of the disk, integrating over all the frequency domain,

$$L_b = \int_0^\infty L_\nu d\nu. \qquad (16)$$

It corresponds to the electromagnetic energy per unit time radiated away in all wavelengths (without including irradiation from the star).

3. RESULTS

In this section we present results of simulations for three different planet luminosities: $L_p = 10^{-5}$, 10^{-4}, and 10^{-3} $L_\odot$. We pay special attention to the gas properties (e.g., density, temperature) and to the spectral consequences of planet feedback for the highest planet luminosity, i.e., $L_p = 10^{-3}L_\odot$.

3.1. Density Field

We first examine how the density profile of the disk is affected by the planet's radiative feedback. We compute the azimuthally averaged density profile $\langle\Sigma\rangle$, given by $\langle\Sigma\rangle = \frac{1}{2\pi}\int_0^{2\pi}\Sigma(r, \phi)d\phi$. In Figure 1 we compare two models: the first one has no feedback ($L_p = 0$), while the second one assumes a planet luminosity of $L_p = 10^{-3}L_\odot$. The density profile are shown at 300 planet orbits. At this stage, the gap carved by the planet is already formed and in a quasi steady state.

For this model, the effects of planet feedback are noticeable in a region of approximately 8 AU radial extent about the planet. We notice that when the feedback is activated, the density profile increases in the inner disk (the disk region inside the planet's orbit), while the density decreases in the outer disk. Outside this region, there is no apparent difference if the planet emits energy or not. The observed changes in the density profile indicate that the planet's luminosity enhances the ability of the disk to transport mass from the outer to the inner disk through the protoplanetary gap. Although not shown here, we have checked that this effect is practically negligible for planet luminosities smaller than $10^{-3}L_\odot$.

In Figure 2, we compare density contours of the disk with and without feedback after 300 planet orbits. As previously
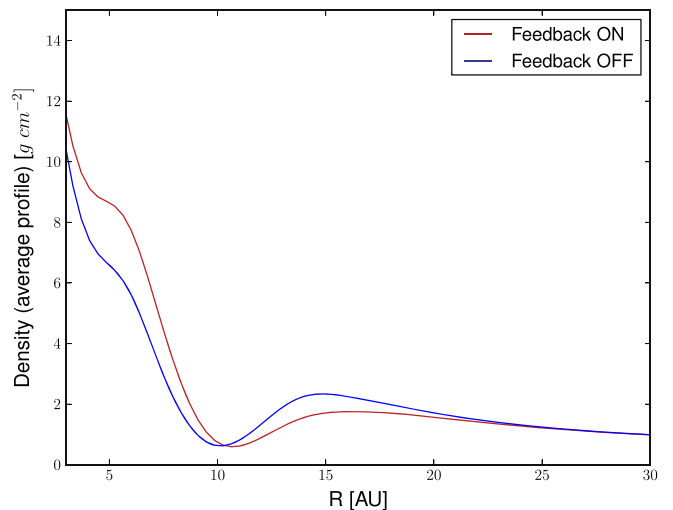
Figure 1. Azimuthally averaged density profiles without and with planet feedback (the planet's luminosity is $L_p = 10^{-3} L_\odot$). Both profiles are displayed after 300 orbits of the planet. Notice that the inner disk accumulates more material when feedback is activated.
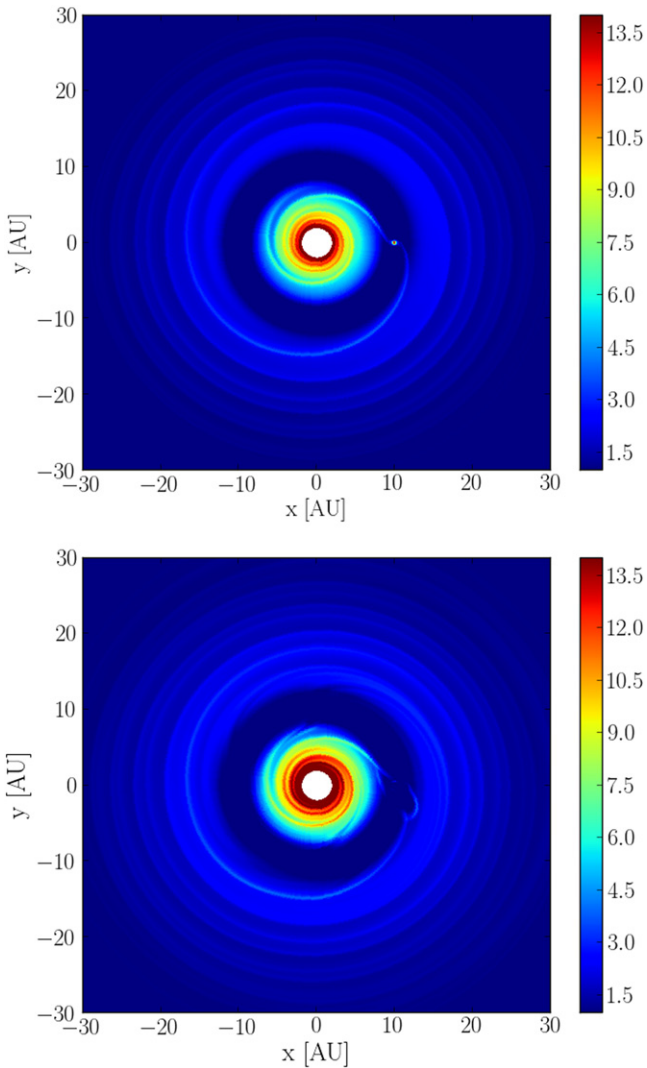
shown by Figure 1, when feedback is activated the inner disk becomes slightly denser, suggesting that the flux of matter from the outer to the inner disk is enhanced by the planet feedback.

It is worth mentioning that, when there is no feedback, only a much smaller increment of the inner disk density is observed as compared with the higher increment when the feedback is activated (Figure 2). Recall that we use *outflow* (inner/outer) boundary conditions, hence the density increment is not a feature of material accumulating at the boundary, but rather a result of a change in the stellocentric flux of matter stimulated near the planet as we will show in Section 3.5. Notice also that in our models there is no material accumulating at the circumplanetary region. On the contrary, material is being slowly evacuated from the CPD (as seen in Figure 2), but after 1000 orbits there is still plenty of material producing an optically thick circumplanetary region. Correspondingly, the density of the outer disk is slightly decreases when the planet feedback is activated. We will show later that actually the disk's stellocentric accretion rate is enhanced at the planet's location, explaining this behavior.

3.2. Temperature Field

In Figure 3 we show the azimuthally averaged temperature profile (i.e., $\langle T\rangle = \frac{1}{2\pi}\int_0^{2\pi}T(r, \phi)d\phi$) of the disk for a model with a planet luminosity of $10^{-3} L_\odot$ and another without feedback, both after 300 orbits of the planet. We see that at the planet's location the azimuthally averaged temperature increases from about 50 K without feedback to nearly 80 K with feedback. Recall that these are *azimuthally averaged* temperature profiles, and do not reflect the large *local* variation shown below.

In Figure 4 we compare the surface temperature of the disk after 300 orbits for the cases with $L_p = 0$ and $L_p = 10^{-3} L_\odot$ (note that a logarithmic scale is used, and that only the inner 20 AU of the disk are shown). When no feedback is included, the maximum temperature occurs at the grid's innermost radius. The maximum temperature reached at the planet's location is about 150 K. When the feedback is activated, a hot

Figure 3. Azimuthally averaged temperature profile without and with feedback ($L_{\rm p} = 10^{-3}\,L_\odot$). Both profiles are taken after 300 orbits of the planet.
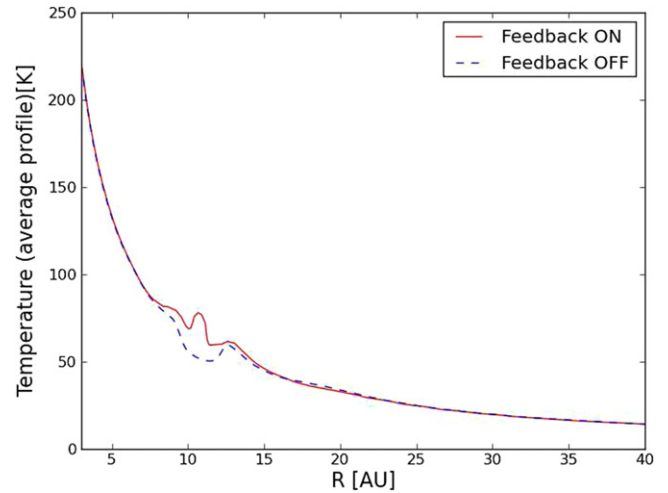
Figure 2. Density contours (cgs units) of the disk at 300 orbits. The top panel shows our results without planet feedback. The bottom panel is for a model with $L_{\rm p} = 10^{-3}\,L_\odot$. When feedback is activated, the inner disk is denser (bottom panel) than without feedback. There is an enhancement of the transport of matter from the outer to the inner disk when feedback is activated. From the figure one can also note that there is no matter accumulating at the circumplanetary region.

spot forms within an AU or so from the planet's location, which is close to the size of the planet's circumplanetary region (recall that in our feedback model, the energy released by the planet is injected in a region of area $\pi R_{\rm CPD}^2$ about the planet's location, where $R_{\rm CPD}$ denotes the radius of the planet's circumplanetary material, which is ~ 0.5 AU). The maximum temperature reached in the planet's CPD is about 1190 K.
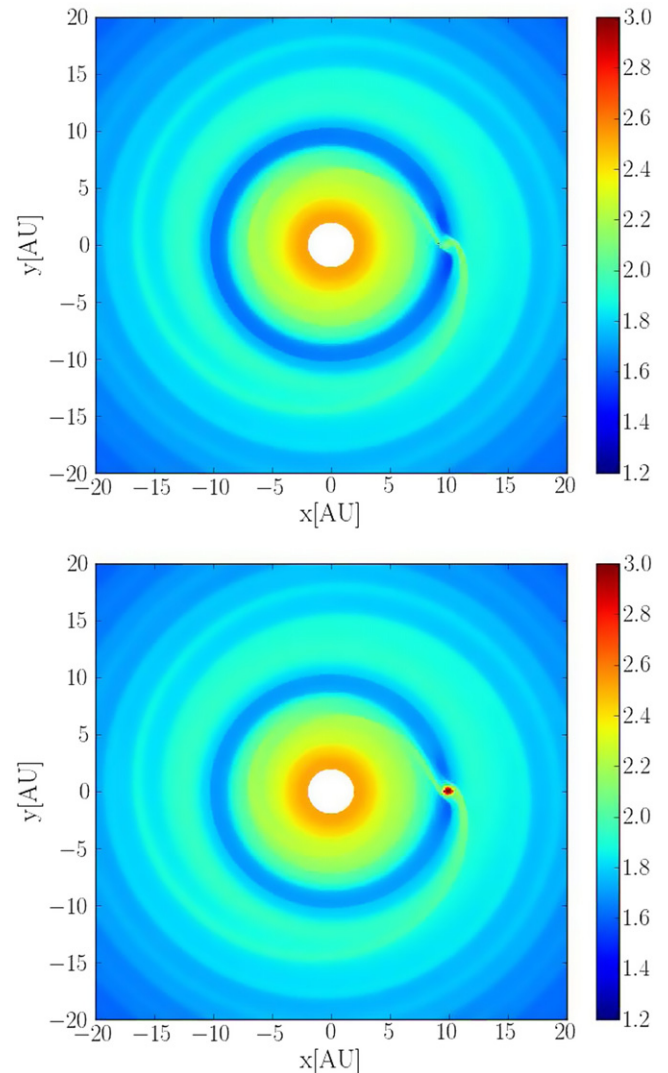
After 300 orbits of the planet, the aspect ratio at the planet's location is about $H_{\rm p}/r_{\rm p} \sim 0.2$, therefore the pressure scale height of the disk at this position is $H_{\rm p} \sim 2$ AU.

3.3. Spectral Signature

We have shown in the previous subsection that the disk temperature near the planet's location is strongly enhanced by the inclusion of the planet feedback. This enhancement (from ~ 100 to ~ 1000 K) should cause a significant variation in the spectral emission of the disk in the vicinity of the planet. In

Figure 4. Effective temperature of the disk after 300 orbits of the planet. The top panel shows our model without planet feedback, the bottom panel is for our model with $L_{\rm p} = 10^{-3}\,L_\odot$. Without feedback, the circumplanetary region reaches temperatures of 160 K, while when the planet luminosity is included this area reaches a peak temperature of about 1190 K.
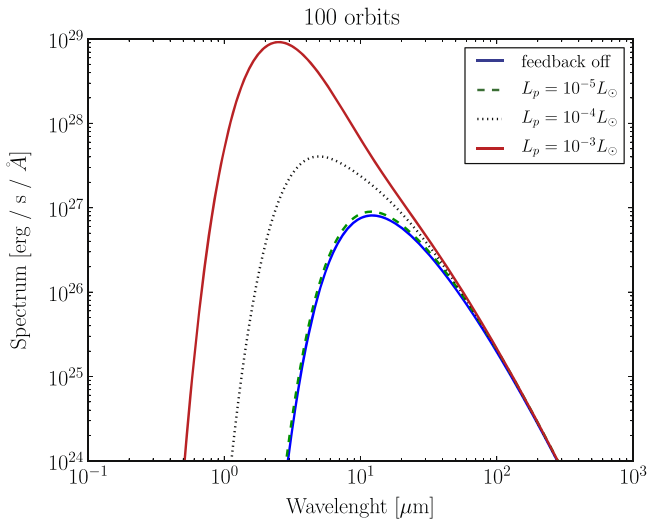
Figure 5. Spectrum of the disk after 300 orbits without and with planet feedback, for $L_p = 10^{-5}$, $L_p = 10^{-4}$ and $L_p = 10^{-3}$ solar luminosities.

Figure 6. Map ratio ($\log_{10}$ scale) of the bolometric emission per unit area between our model with $L_p = 10^{-3} L_\odot$ and our model with $L_p = 0$, at 300 orbits. When the feedback is activated, the bolometric surface brightness is about $10^{3.6}$ times higher in the circumplanetary region, and there is also an excess of emission along the planet's orbit.
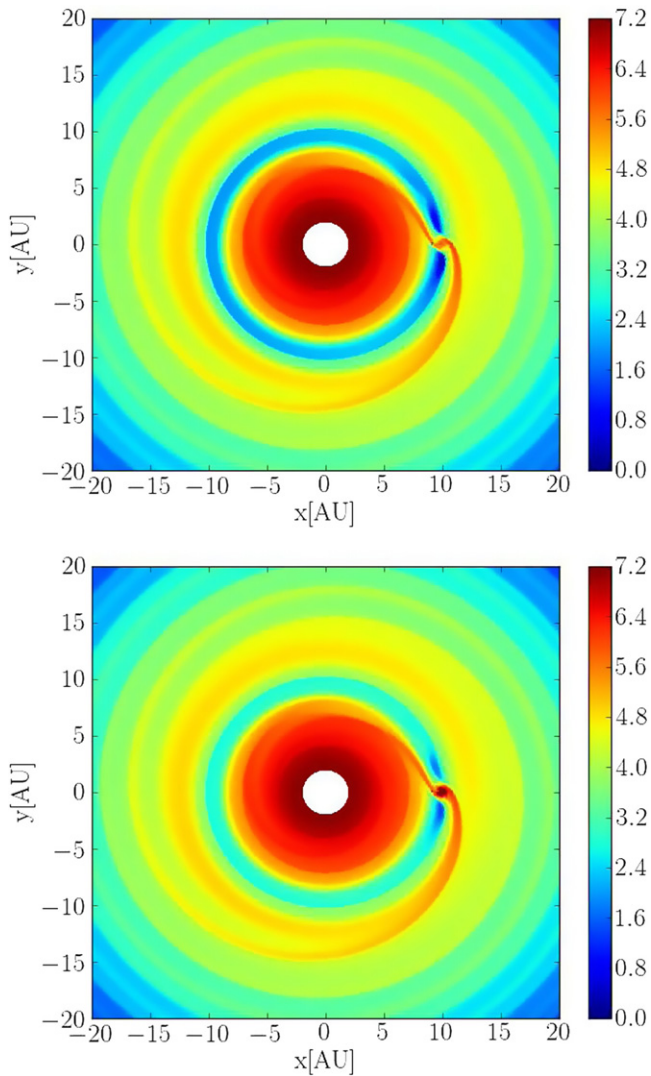
Figure 5 we display after 300 orbits how the disk spectrum, calculated from Equation (15), changes for different planet luminosities ($L_p = 10^{-5}$, $L_p = 10^{-4}$, $L_p = 10^{-3}$, and $L_p = 0$ $L_\odot$). We see that the spectrum is dramatically modified when the feedback is higher than $L_p \gtrsim 10^{-4} L_\odot$.

At the planet's location the disk temperature without feedback is about 150 K. When the feedback is included, the temperature derived from the energy equation in the vicinity of the planet peaks at 1100 K[6] for planet luminosities $L_p \gtrsim 10^{-3} L_\odot$. This increase in temperature produces a corresponding increase in the peak flux density by a factor of ~ 100, as seen in Figure 5. Notice also that without feedback the spectrum of the disk peaks at 19.3 μm, and that for a planet luminosity of $L_p = 10^{-3} L_\odot$, the spectrum peaks at 2.5 μm.

Using Equation (16), we can integrate the spectrum from Figure 5 to obtain the bolometric luminosity of the entire disk.[7] In the simulation without feedback, the bolometric luminosity is $L_b = 5.54 \times 10^{-2} L_\odot$, while in the case when we assume a planet luminosity of $L_p = 10^{-3} L_\odot$, the bolometric luminosity increases to $L_b = 0.98 L_\odot$. In other words, the radiative feedback from the planet results in a disk luminosity increased by a factor of 17.8.

To better appreciate the differences between the cases $L_p = 0$ and $L_p = 10^{-3} L_\odot$, we plot in Figure 6 (log scale) the ratio between the bolometric emission per unit area (given by $\int_0^\infty \Phi(T(r, \phi)) d\lambda = \sigma T^4$) for $L_p = 10^{-3} L_\odot$ and the emission when $L_p = 0$, after 300 orbits of the planet. From Figure 6 we notice that when the feedback is activated, the blackbody emission (σT^4) in the vicinity of the planet, inside a radius of about ~ 5 AU, increases by up to 3.6 orders of magnitude over

a situation without feedback. Also, we notice that along the orbital path of the planet around the central star, the feedback leaves a "track" of disk surface brightness enhanced by about one order of magnitude. This track indicates that the radiative feedback from the luminosity of the planet induces net heating of the gas not only in the close vicinity of the planet, but also along the planet's trajectory.

In Figure 7, we display at 300 planet orbits the blackbody radiation $B_\lambda(T(r, \phi))$ for $\lambda = 2.5 \mu$m for the cases without and with feedback ($L_p = 10^{-3} L_\odot$). The feedback dramatically increases the blackbody radiation in the circumplanetary region. We point out that there could appear to be an energy conservation problem here, because when there is no feedback we get a luminosity output from the entire disk of about $L_b = 5.5 \times 10^{-2} L_\odot$, while by adding a relatively small source of $L_p = 10^{-3} L_\odot$, we obtain an output luminosity of $0.98 L_\odot$. In the next subsection, we run several tests in order to check this result, concluding that there is no inconsistency with energy conservation. The additional energy comes from an increase in the stellocentric accretion rate through the disk when the feedback is activated, as will be explained in Section 3.5 below.

3.4. Feedback Behavior for Other Viscosity Prescriptions

In this section we examine to what extent the impact of the planet's radiative feedback depends on the assumption about the viscosity prescription. For this purpose, we have carried out a number of simulations with different viscosity prescriptions.

We first employed alpha viscous disk models. The alpha disk model, as it is implemented in the public release of FARGO-AD, assumes a kinematic viscosity $\nu = \alpha \langle c_s^2 / \Omega \rangle$ where the brackets stand for the azimuthal average. In other words, the kinematic viscosity is purely radial. We have carried out simulations with $\alpha = 4 \times 10^{-4}$, 4×10^{-3}, and 4×10^{-2}, and found nearly identical peak temperature in the planet's circumplanetary region. Our results are listed in Table 1, along

---

[6] We point out that the high temperatures we observe in our numerical models are also recovered by Zhu (2015). In his one-dimensional accretion disk models, the temperature down at the atmosphere of the planet ($r \sim R_J$) reaches ~ 2000 K, without invoking any energy input from the planet itself. Notice that those scales cannot be resolved with our numerical scheme, so a direct comparison is not possible.

[7] Notice that this bolometric luminosity does not include the emission from the star. Moreover, the quoted values depend on the radial extent of the disk, most importantly on its inner radius, which we set for numerical convenience to 1 AU.

Figure 7. Local blackbody flux per unit area $B_\lambda(T(r, \phi))$ of the disk according to Equation (14), taking $\lambda = 2.5 \, \mu$m. The map is in log scale and the units are erg s^{-1} cm^{-3}. The upper panel corresponds to a model without feedback, the bottom panel is for $L_{\rm p} = 10^{-3}L_\odot$. The highest surface brightness comes from the planet's circumplanetary region.

with the disk's accretion rates at the planet's location, which we will detail in the next section.

Lastly, we ran an inviscid model, i.e., a model without shear viscosity ($\nu = 0$; note, however, that this model still includes artificial viscous heating via a bulk viscosity, as in all the models presented in this paper—see the model described in Section 2.3.1). In that case, we find again a peak temperature near the planet of 1166 K, which is very similar to the cases presented before with different viscosity prescriptions. All these numerical experiments show that the peak temperature that we find with planet feedback activated is basically independent of the disk's viscosity.
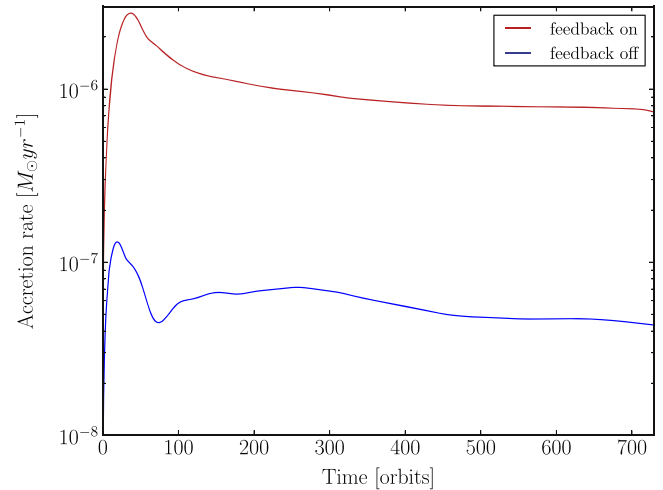
3.5. Accretion Rate

We have shown in Section 3.3 that the bolometric luminosity of the disk increases by a factor of ~20 with planet feedback and a planet luminosity of $L_{\rm p} = 10^{-3}L_\odot$, compared to a disk without planet feedback. This excess of energy mostly arises from the planet's circumplanetary region and from a narrow

Table 1
Peak Temperature and Disk Accretion Rate Values at the Circumplanetary Region for Different Viscosity Prescriptions

Viscosity model	$T_{\rm peak}^{\rm on}$ (K)	$T_{\rm peak}^{\rm off}$ (K)	$\dot{M}_{\rm on}(M_\odot \, {\rm yr}^{-1})$	$\dot{M}_{\rm off}(M_\odot \, {\rm yr}^{-1})$
$\alpha = 4 \times 10^{-4}$	1170	125	3.7×10^{-6}	2×10^{-8}
$\alpha = 4 \times 10^{-3}$	1190	200	2.6×10^{-6}	1.2×10^{-7}
$\alpha = 4 \times 10^{-2}$	1200	276	3.8×10^{-6}	2.3×10^{-7}
$\nu = 0$	1166	100	1×10^{-6}	1×10^{-8}

Note. With feedback (Columns 2 and 4, $L_{\rm p} = 10^{-3} L_\odot$) and without feedback (Columns 3 and 5).

Figure 8. Disk accretion rate at the planet's orbital radius, defined by Equation (17), without and with ($L_{\rm p} = 10^{-3} L_\odot$) planet feedback. With feedback the accretion rate at the planet's orbital radius is enhanced by an order of magnitude. The peak of the accretion rate is reached near ~40 planet orbits; at this stage the temperature reaches a maximum near the planet's vicinity.

region about the planet's orbital radius (see Figure 6). The luminosity can be related to an accretion rate; an excess of luminosity should therefore have a corresponding increase in the disk's accretion rate.

We calculate the azimuthally integrated accretion rate of the disk at the planet's location as

$$\dot{M} = \int v_r(r_{\rm p}, \phi)\Sigma(r_{\rm p}, \phi)r_{\rm p}d\phi, \qquad (17)$$

where v_r is the radial velocity of the gas. In Figure 8 we display the time evolution of $\dot{M}$ for two models: one with feedback ($L_{\rm p} = 10^{-3}$) and one without feedback ($L_{\rm p} = 0$), assuming an alpha disk with $\alpha = 4 \times 10^{-3}$ (our fiducial model). We see that, when the feedback is activated, the disk's accretion rate is enhanced by an order of magnitude. The accretion rate reaches similar values for different viscosity models, see Table 1.

We notice from Figure 1 that the density average at the planet's location did not differ much between the cases with and without feedback, hence, in order to have an enhancement of the accretion rate at that region, it must be the radial velocity that is enhanced. This is exactly what we see in Figure 9, where the radial velocity is enhanced by a factor of ~4 when the feedback is activated. It is not expected to have a similar enhancement factor to that observed for the accretion rate mentioned above (i.e., one order of magnitude) because
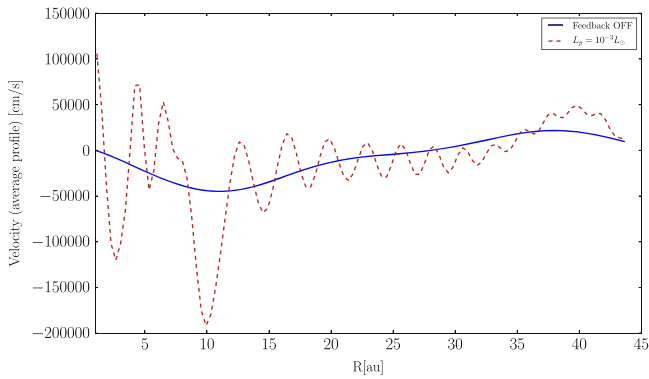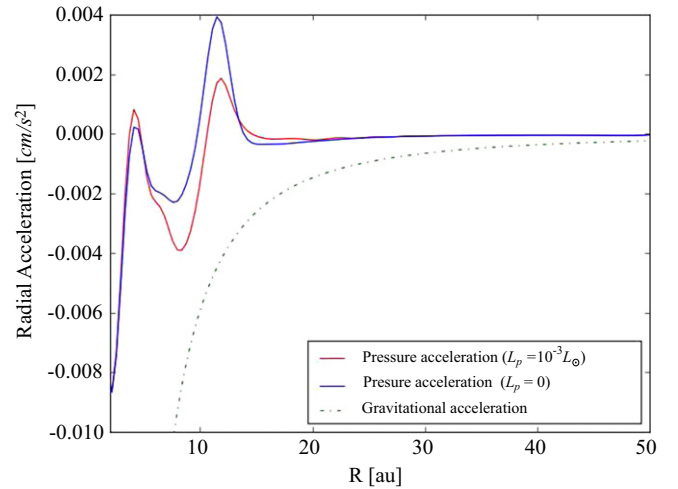
Figure 9. Azimuthal average of the radial velocity after 600 orbits. When the feedback is activated, the radial velocity is enhanced by a factor of ~4 at the planet's location (10 AU).

Figure 10. Azimuthal average of the radial acceleration due to the pressure work done by the disk without and with feedback. The gravitational radial acceleration is displayed for comparison.

Figures 1 and 9 show an *azimuthally averaged* radial velocity, rather than local values at the planet's location. To compute $\dot{M}(r_p)$ as indicated in the preceding paragraph we use local values (where, for instance, the density takes larger values at r_p than the azimuthally averaged value), then we integrate over the azimuthal coordinate.

At the end of Section 3.3, we discuss the fact that our simulations show, for instance, that when we use a local energy input of $L_p = 10^{-3} L_\odot$, we obtain an energy output of $L_b \sim L_\odot$. This could be misinterpreted as a non-conservative evolution of the energy. To show that this is not the case, we argue that the origin of the extra energy comes from an increase in the disk's accretion rate stimulated by the feedback of the planet, and that this enhancement is independent of the viscosity prescription.

When radiation feedback is active, the luminosity of the disk at the location of the planet is proportional to the stellocentric disk accretion rate (which attains a maximum value), i.e., $L_{acc} \propto \dot{M}$ at R_p. For instance, taking the model with $\alpha = 4 \times 10^{-3}$, the accretion rate at 300 orbits is $\dot{M}^{on} \approx 10^{-6} M_\odot \text{ yr}^{-1}$ with feedback, and $\dot{M}^{off} = 6 \times 10^{-8} M_\odot \text{ yr}^{-1}$ without (see Figure 8). From this, we find that the accretion luminosity of the disk should be increased by a factor of roughly $L_{acc}^{on}/L_{acc}^{off} = \dot{M}^{on}/\dot{M}^{off} \simeq 17$ by the inclusion of planet feedback. This is indeed in good agreement with the increase in bolometric luminosity calculated in Section 3.3, where the luminosity increase is found to be ≈ 17.8. Our results clearly show that there is no imbalance in the energy bill during the simulation, and that the extra energy is the direct product of an enhancement in the disk accretion rate, which in turn was stimulated by the planet feedback.

Now we briefly describe the effect on the disk dynamics when the radiative feedback of the planet is included. From a dynamical point of view, the radial component of the Navier–Stokes equation includes the radial pressure gradient of the fluid (the term $(1/\Sigma)\partial P/\partial r$). A local enhancement of this term at the planet's location should lead to a local increase in the radial velocity (understood in absolute value). In Figure 10, we compare the azimuthally averaged radial acceleration due to the gradient pressure when the feedback is turned on $(L_p = 10^{-3}L_\odot)$ and off, after 100 planet orbits. We show for comparison the radial gravitational acceleration due to the central star. We see that the pressure gradient is particularly strong near the planet's location, as expected. Moreover, with

feedback the radial acceleration is more negative, which acts to increase the accretion rate through the disk near the planet's location, as seen before.

Similar conclusions were obtained by Owen (2014), who constructed a 1D radial "transition" disk model including feedback from the protoplanet acting over the gas and dust components of the disk. He included the radial and azimuthal accelerations of the dust particles produced by radiative feedback from the planet in a secular model of a protoplanetary disk with an embedded accreting planet (e.g., Clarke & Pringle 1988), finding that the accretion rates observed in transition disks are better explained when the radiative feedback of the planet is included. The Owen (2014) model assumes azimuthal symmetry, in which the radiation feedback and the disk–planet interaction are treated as average quantities. By contrast, our model is non-axisymmetric (2D), and we include a non-stationary energy equation to introduce the radiative feedback.

It is important to clarify that this accretion enhancement should lead to a transient situation explained as this: as shown above, the local feedback promotes the flux of matter in a region close to the CPD. As seen in Figure 2, gas density slowly diminishes at the CPD. If this continues long enough, the CPD will be depleted, becoming optically thin. If this happens, radiation from the planet will no longer interact with the gas, escaping immediately from the disk without heating it. Therefore, the radiative feedback will no longer affect the CPD, muting its effect on the gas dynamics. Consequently, there will be no more accretion enhancement or extra luminosity produced. Once the CPD starts resumes accumulation of material and becomes optically thick again, radiation feedback will interact once more with the gas, modifying its dynamics as before. From our calculations, to deplete the CPD with a planet feedback of $\sim 10^{-3} L_\odot$ located at 10 AU takes more than 10000 years, but further investigations are needed to clarify this point.

To summarize, our findings show that a relatively small source of heating coming from the planet's circumplanetary region will induce enhanced disk accretion rates near or around the planet's orbital radius. This enhancement facilitates the extraction of gravitational energy, which locally heats the gas, enhancing the luminosity in the circumplanetary region. This

local increase in the disk temperature then leads to an increase in the accretion rate, increasing the temperature even further (and thus the luminosity). This effect results in a positive feedback until a thermal balance is reached where the heat dissipation rate equals the radiative cooling rate ($Q^+ = Q^-$ in our notation).

These accretion luminosities should be detectable inside gaps. It should be noticed that it is not the intrinsic luminosity of the planet, but a local gas luminosity stimulated by the action of the planet feedback. In the next subsection, we present results of hydrodynamical simulations dedicated to interpreting the observations of a protoplanet candidate around star HD 100546.

3.6. HD 100546 Simulation

A protoplanet injecting extra local heating in the disk via the feedback mechanism explained in the previous sections could explain the bright compact emission detected in the L' band with NACO in the disk of HD 100546 (Quanz et al. 2013a). HD 100546 is a Herbig Ae/Be star which harbors a protoplanet candidate orbiting at 68 AU (Quanz et al. 2013b; Currie et al. 2014). Motivated by these observations, we have carried out a set of simulations for HD 100546. We compare the results of various accretion luminosities with the luminosity of the observed planet candidate.

Based on interferometric data using AMBER/VLTI and photometric observations, Tatulli et al. (2011) proposed a disk model for the circumstellar environment of HD 100546. Using this model we adopt a disk scale height profile $H(r) = 12 \, (r/100 \, \mathrm{AU})^{1.1} \, \mathrm{AU}$, and a surface density profile $\Sigma(r) \propto r^{-1}$ as initial conditions for our simulations. We tailor the disk mass in order to guarantee that the circumplanetary region remains optically thick. We thus set the disk gas mass to $M_d = 15 \times 10^{-2} M_\odot$ (while Tatulli et al. 2011 reported $5 \times 10^{-2} M_\odot$ for gas). From Panić et al. (2010), we assume a central star of mass $M_\star = 2.5 M_\odot$ (which defines our unit of mass), implying a planet's orbital period of 354.6 years. Neither irradiation nor flux diffusion from the central star is taken into account in our simulation. In Section 4.1, we justify this approximation for the irradiation through a simple analytical calculation. As in our fiducial model, the disk is treated as an alpha viscous disk with $\alpha = 4 \times 10^{-3}$.

The planet is located at $r_p = 68$ AU, which is taken as the code's unit of length. For numerical convenience, the grid now extends from 10 to 200 AU along the radial direction, which corresponds to radii ranging from 0.15 to 3.0 in code units.

Informed by our dust model for HD 100546 (see Section 3.6.1 below), we changed the opacity prescription in our feedback calculation, taking into account an average opacity for a mix of dust species given by $\kappa = 130 \, \mathrm{cm^2 \, g^{-1}}$. This is more adequate for transition disks such as HD 100546.

We carried out a set of simulations with various planet luminosities: $L_p = \{0; 2.5; 5\} \times 10^{-4} L_\odot$. The observed emission in the L' band is thought to correspond to a protoplanet with a mass between 1 and 8 M_J (Quanz et al. 2013a). We fix the planet mass to $M_p = 5 M_J$. Our results of simulations are shown after 600 planet orbits, or 24.2×10^3 years (as in the previous sections, the planet's mass reaches its imposed value over ten orbital periods).

We show in Figure 11 contours of the disk temperature for the different planet luminosities mentioned above. The

coordinates in the figures are in code units, therefore the planet (at 68 AU) appears at $r = 1$.

The top panel corresponds to a simulation without feedback. In this case, the hottest temperatures come from the innermost region of the disk (200 K). The circumplanetary region reaches a maximum temperature of about 80 K. The middle panel shows a model with feedback and a planet luminosity $L_p = 2.5 \times 10^{-4} L_\odot$. In this case, the protoplanet region peaks at 270 K. In the lower panel, $L_p = 5 \times 10^{-4} L_\odot$, which gives a peak temperature (at the planet's location) of 325 K.

By integrating the spectrum over the whole disk surface and over the entire wavelength range (Equation (16)), we obtain the bolometric luminosity of the disk. Without feedback, it yields $L_b^{\mathrm{off}} = 4.2 \, L_\odot$. For $L_p = 2.5 \times 10^{-4} L_\odot$, we obtain a disk luminosity of about $L_b = 4.7 \, L_\odot$, resulting in a disk 1.1 times brighter than without feedback (i.e., $L_{\mathrm{on}}/L_{\mathrm{off}} = 1.1$). This can be explained by the fact that the addition of a small source of heating near the planet (associated with $L_p = 2.5 \times 10^{-4} L_\odot$) locally enhances the disk accretion rate at the planet's location, and results in a positive feedback able to produce a disk that is $\sim$10% brighter than without feedback. We point out that the disk luminosity without feedback is 4.3 solar luminosities (for a disk extending from 10 to 200 AU), which is consistent with the bolometric luminosity of $\sim$10 $L_\odot$ reported by Benisty et al. (2010) (for a disk from 10 to 500 AU). Recall that we neglect irradiation from the star, and that modeling a smaller than observed disk is likely to explain the factor of $\sim$2 discrepancy.
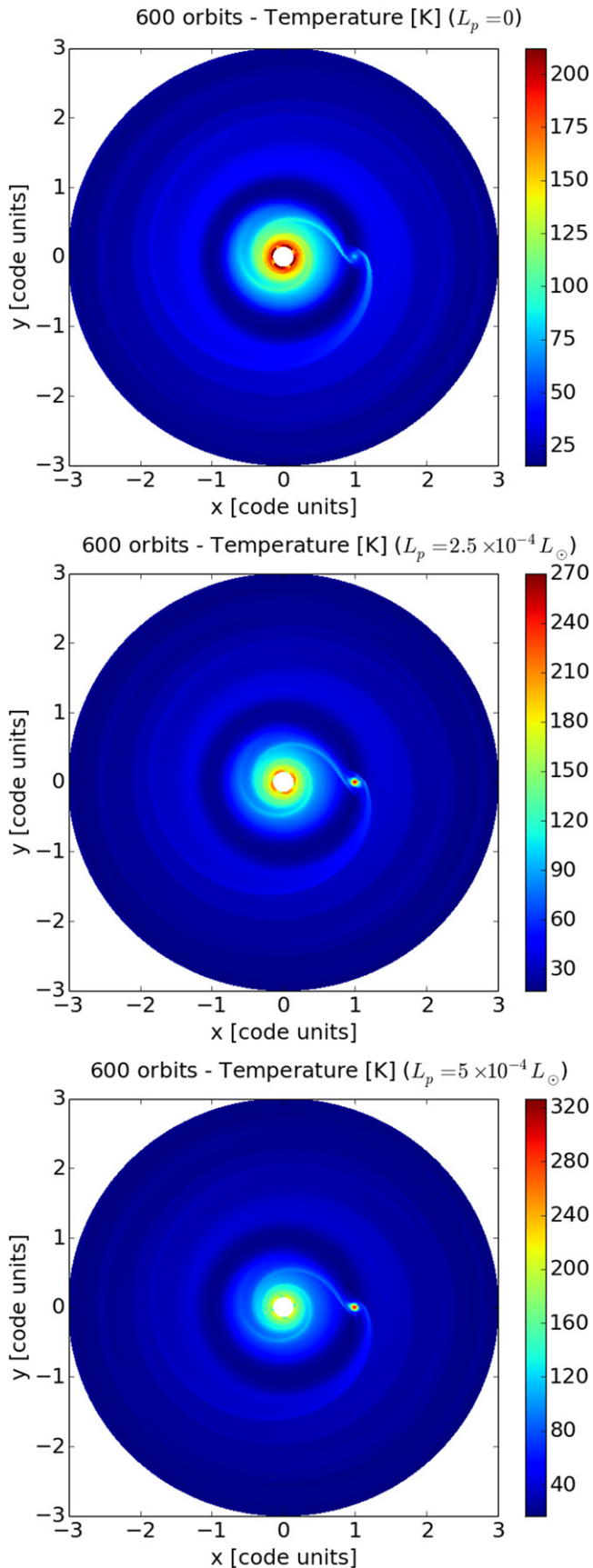
3.6.1. Radiative Transfer

In order to compare our HD 100546 simulation with the L' observations from Quanz et al. (2013b), we input the hydrodynamical gas density and gas temperature fields into the RADMC3D[8] radiative transfer code (version 0.38, Dullemond et al. 2014). At IR wavelengths the emission is dominated by thermal and scattered emission from micron-sized dust. Small grains should be well mixed, hence we assume that the dust distribution follows the same density field as the gas in the simulation. These grains should account for the bulk of the L' emission.

Our model dust distribution consists of a mix of two common species: amorphous carbons and astronomical silicates (Draine & Lee 1984). As informed by previous modeling of spectral energy distribution (Benisty et al. 2010, Tatulli et al. 2011), our grain size distribution follows a power law with exponent -3.5, and particle sizes ranging from 0.05 to 1000 μm. We used Mie theory (homogeneous spheres) to compute the dust opacities for anisotropic scattering. The optical constants were taken from Li & Greenberg (1997) for amorphous carbon grains, and from Draine & Lee (1984) for silicates. The intrinsic densities of the grains are 2 and 4 g cm^{-3} for amorphous carbons and silicates, respectively. We also assume $T_{\mathrm{gas}} = T_{\mathrm{dust}}$.

The 2D surface densities for each dust species are extended vertically following hydrostatic equilibrium. This produces a 3D volume with a Gaussian profile in the vertical direction. The scale height of the disk is assumed to be the same for both dust species and it is set by the temperature field through the relation $H(r) = \sqrt{\gamma \, \overline{R} \, T(r)} \, r / v_{\mathrm{Kep}}$, where v_{Kep} is the Keplerian

---

[8] http://www.ita.uni-heidelberg.de/~dullemond/software/radmc-3d/

Figure 11. Contours of the disk temperature after 600 planet orbits. From top to bottom: $L_p = 0$, $L_p = 2.5 \times 10^{-4} L_\odot$, and $L_p = 5 \times 10^{-4} L_\odot$. The peak temperature near the planet is 80, 270, and 325 K, respectively.

velocity. For simplicty the temperature was assumed constant in the vertical direction. A better vertical description of the temperature would require a full account of stellar irradiation and stellar flux diffusion in the simulations. The final image is produced by performing a second-order volume ray-tracing method. The results of our radiative transfer calculation for L' are shown in Figure 12.

Quanz et al. (2013b) calculated the luminosity of the hot spot around the companion candidate HD 100546b, assuming a point source embedded in a region 0.1 arcsec in size ($\sim$10 AU) located at 68 AU from the central star, reporting an apparent L' magnitude of 13.2, which translates into a flux density of 1.3 mJy. In order to compare with our planet feedback predictions, we computed the emergent flux from the vicinity of the protoplanet in the same way.

The simulation including an embedded protoplanet with an accretion luminosity of $L_p = 2.5 \times 10^{-4} L_\odot$ yields an emerging flux from the circumplanetary vicinity of 0.7 mJy in L'. On the other hand, an accretion luminosity of $L_p = 5 \times 10^{-4} L_\odot$ already produces a flux density of $\sim$3 Jy, about two times higher than the flux levels reported by Quanz et al. (2013b).

A key result from our model is that the emitted luminosity from the protoplanet region depends on the prescribed feedback and not on the viscosity prescription. Therefore, from our simulations for HD 100546b, we conclude that the protoplanet candidate is compatible with an accreting object of about five Jupiter masses, with a planet luminosity of about $\sim$2.5 $\times$ 10^{-4} $L_\odot$.

4. DISCUSSION

### 4.1. Irradiation from the Central Star

Here we briefly discuss the possible effect of the irradiation from the central star on the disk. The flux penetrating the surface of the disk can be calculated as (see for instance Frank et al. 2003)

$$F_{\rm irr} = (1 - \beta) \frac{L_\star}{4\pi r^2} \cos \varphi, \qquad (18)$$

where β is the albedo (reflection coefficient), and ϕ is the angle formed by the incident radiation and the normal to the surface. It can be shown that $\cos \varphi \simeq dH/dr - H/r$, and using $F_{\rm irr} = \sigma T_{\rm irr}^4$, we can compute the irradiation temperature $T_{\rm irr}$ at the surface of the disk as

$$T_{\rm irr}^4 = \frac{L_\star}{4\pi r^2 \sigma} \left(\frac{H}{r} \right) \left(\frac{d \ln H}{d \ln r} - 1 \right) (1 - \beta). \qquad (19)$$

From analytic (Chiang & Goldreich 1997) and numerical solutions (D'Alessio et al. 1998; Dullemond et al. 2002), it can be shown that the height H of the disk when stellar radiation is taken into account has a power-law dependence with radius, $H \propto r^f$, with $f \approx 1.3-1.5$. Using these values, we obtain that ($d \ln H/d \ln r - 1$) varies slightly between 0.3 and 0.5. The aspect ratio (H/r) can reach values from 10^{-4} to 10^{-1} (e.g., Bell et al. 1997). Even taking values that give the maximum temperature from the above equation, i.e., $d \ln H/d \ln r - 1 = 0.5$, $H/r = 10^{-1}$, and $\beta = 0$ (all radiation penetrates), and assuming a central star of 50 $L_\odot$ (Panić et al. 2010 quote 26 $L_\odot$ for HD 100546), the disk temperature
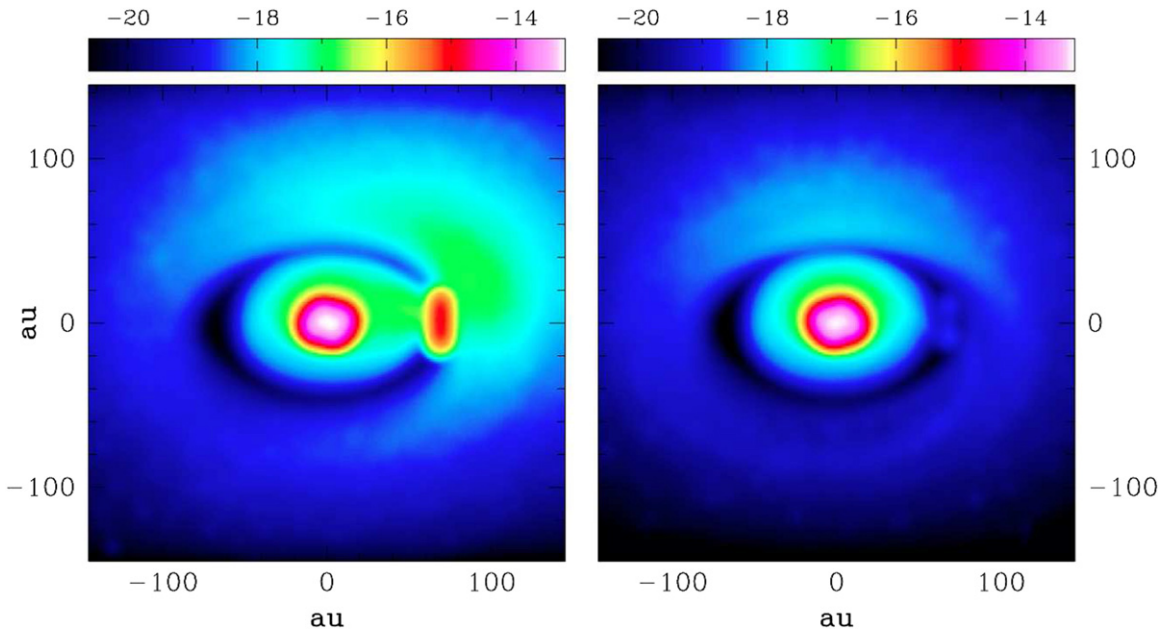
Figure 12. Radiative transfer predictions in the L' band (3.8 μm), for a disk inclination angle of 47°, calculated on the density and temperature fields shown in Figure 11. The left panel shows the results with radiative feedback ($L_p = 2.5 \times 10^{-4}\,L_\odot$), the right panel shows the case without feedback. The radiative feedback results in a circumplanetary hotspot reaching ∼1 mJy in L', close to the 1.3 mJy observed by Quanz et al. (2013b). The inclusion of the inner disk (with radius <10 AU) would result in a bright stellar point source, which could efficiently be cancelled by angular differential imaging (ADI). The images have been convolved with a 0.1 arcsec Gaussian PSF. Color stretch is logarithmic. Images are in units of erg cm^{-2} s^{-1} sr^{-1}.

from irradiation at $r = 68$ AU reaches ∼60 K, while from viscous dissipation plus radiative feedback the temperature reaches values $\gtrsim$100 K depending on the planet luminosity L_p.

For the simulations with a solar-type star presented in Sections 3.1–3.5, we obtain a surface temperature of about ∼55 K at $r = 10$ AU (planet's location). Therefore, the heating of the disk by the central star is, in the most extreme case, of the same order as the temperature obtained by viscous dissipation when there is no feedback ($T \sim 55$ K), and one order of magnitude below when the feedback is activated $T \sim 1000$ K (see Figure 4).

We conclude from this that the surface temperature in our 2D disk model is not expected to be affected by the irradiation energy of the central star, and that this effect can be neglected in our calculations.

4.2. Application to Massive Black Hole Binaries

Even though in this paper we focus on protoplanetary disks, a very similar physical set-up is that of unequal-mass massive black hole binaries. Such binaries are expected to form after galaxy mergers, once the central massive black hole of each galaxy migrates to the center of the new system due to dynamical friction (e.g., Begelman et al. 1980). During the merger, large quantities of gas get funnelled to the inner region of the new galaxy, where they form a nuclear gas disk that interacts with the binary (e.g., Mayer et al. 2007). If the masses of the black holes are dissimilar, the secondary will orbit the primary, while both are embedded in the gaseous disk, in a situation very much resembling the star–planet–disk systems we model in this paper (e.g., Armitage & Natarajan 2002), especially considering that both planets and embedded black holes are expected to produce luminosity by accretion.

Binaries with separations of a few parsecs or less are not directly resolvable, so we need to rely on indirect methods to identify them. One such method is based on the assumption that the gaseous disk around the primary radiates as a multicolor blackbody. If the secondary produces a gap in the disk, then the spectrum will show a dip at the wavelength range associated with the temperature of the missing gas (Chang et al. 2010; Gültekin & Miller 2012). Extrapolating our results to that regime, it is clear that the disk spectra will also be modified by the heating-up of the gas surrounding the secondary black hole, likely producing a larger dip and a concurrent increase of the shorter wavelength emission. A more detailed analysis of this situation is deferred to a follow-up paper.

5. SUMMARY

In this paper we present 2D hydrodynamical simulations of the interaction between a Jupiter-mass planet and its parent protoplanetary disk, including for the first time the effect of the planet's radiative feedback onto the disk (energy released by the planet as it assembles its mass). In this first work, we assume that the energy released by the planet to the disk is constant over the duration of our simulations, a few hundred planet orbits typically. We carried out various simulations, taking realistic parameters for protoplanetary disks that could be identified with actually observed systems, such as, e.g., HD 100546 (Quanz et al. 2013a; Currie et al. 2014), varying the luminosity of the planet.

We find that planet luminosities below $L_p \lesssim 10^{-4}L_\odot$ barely modify the disk response to the planet: the gap formed by the planet does not show any noticeable modification compared to the case without feedback and the emitted spectrum of the disk remains practically unchanged. However, planets with

$L_p \gtrsim 10^{-4} L_\odot$ introduce significant changes: the additional energy input from the planet heats up the disk, locally enhancing the local disk accretion rate (understood into the primary), increasing even more the temperature at this location. This mechanism results in a positive feedback magnifying the energy output until a thermal balance is reached.

Figure 8 shows the increase in the disk accretion rate in the planet's vicinity. The spectrum and luminosity of the disk are modified, shifting the emissions to higher amplitudes and shorter wavelengths. For instance, assuming $10^{-3} L_\odot$ for the planet feedback, the accretion rate in the planet's vicinity increases from 6×10^{-8} (without feedback) to $10^{-6} M_\odot \, \mathrm{yr}^{-1}$, and translates into an increase in the disk luminosity from $L_{\mathrm{disk}} = 5.5 \times 10^{-2} L_\odot$ (without feedback; $\lambda_{\mathrm{peak}} = 19.3 \, \mu\mathrm{m}$) to $L_{\mathrm{disk}} = 0.9 \, L_\odot$ ($\lambda_{\mathrm{peak}} = 2.5 \, \mu\mathrm{m}$).

We find that our results do not depend on the viscosity prescription. Thus, in our models, setting the planet luminosity will fix the accretion rate, temperature and luminosity in a region close to the planet. Our results imply that observations of protoplanetary disks where planets are formed could reveal the accretion process onto them, without much interference from nuance parameters such as the viscosity.

Finally, we build a model for the system around HD 100546 (Quanz et al. 2013b), reproducing quite well the observed flux density in the L' band of 1.3 mJy from the region around the accreting candidate planet HD 100546b. Our model indicates that this system contains a forming planet with a luminosity of $\sim 10^{-4} L_\odot$.

REFERENCES

Armitage, P. J., & Natarajan, P. 2002, ApJL, 567, L9
Baruteau, C., & Masset, F. 2008, ApJ, 678, 483
Bate, M. R., Lubow, S. H., Ogilvie, G. I., & Miller, K. A. 2003, MNRAS, 341, 213
Begelman, M. C., Blandford, R. D., & Rees, M. J. 1980, Natur, 287, 307
Bell, K. R., Cassen, P. M., Klahr, H. H., & Henning, Th. 1997, ApJ, 486, 372
Bell, K. R., & Lin, D. N. C. 1994, ApJ, 427, 987
Benisty, M., Tatulli, E., Ménard, F., & Swain, M. R. 2010, A&A, 511, A75
Biller, B. A., Males, J., Rodigas, T., et al. 2014, ApJL, 792, L22
Casassus, S., Perez, M., Jordán, S., et al. 2012, ApJ, 754L, 31C
Casassus, S., van der Plas, G. M., Perez, S., et al. 2013, Natur, 493, 191
Chang, P., Strubbe, L. E., Menou, K., & Quataert, E. 2010, MNRAS, 407, 2007
Chiang, E. I., & Goldreich, P. 1997, ApJ, 490, 368
Clarke, C. J., & Pringle, J. E. 1988, MNRAS, 235, 365
Close, L. M., Follette, K. B., Males, J. R., et al. 2014, ApJL, 781, 30
Crida, A., Baruteau, C., Kley, W., & Masset, F. 2009, A&A, 502, 679
Currie, T., Muto, T. , Kudo, T., et al. 2014, ApJL, 796, L30
D'Alessio, P., Canto, J., Calvet, N., & Lizano, S. 1998, ApJ, 500, 411
D'Angelo, G., Kley, W., & Henning, T. 2003, ApJ, 599, 548
Draine, B. T., & Lee, H. M. 1984, ApJ, 285, 89
Frank, J., King, A., & Raine, D. 2003, Accretion Power in Astrophysics (3rd ed.; Cambridge: Cambridge Univ. Press)
Gültekin, K., & Miller, J. M. 2012, ApJ, 761, 90
Hubeny, I. 1990, ApJ, 351, 632
Kley, W., D'Angelo, G., & Henning, T. 2001, ApJ, 547, 457
Li, A., & Greenberg, J. M. 1997, A&A, 323, 566L
Mamajek, E. E. 2009, AIP Conf. Proc.1158, Exoplanets and Disks: Their Formation and Diversity, Usuda , T., Tamura, M., & Ishii, M., 3
Marley, M. S., Fortney, J. J., Hubickyj, O., Bodenheimer, P., & Lissauer, J. J. 2007, ApJ, 655, 541
Masset, F. 2000, A&AS, 141, 165
Mayer, L., Kazantzidis, S., Madau, P., et al. 2007, Sci, 316, 1874
Morbidelli, A., Szulágyi, J., Crida, A., et al. 2014, Icar, 232, 266
Mordasini, C. 2013, A&A, 558, 1
Nayakshin, S. & Cha, S.-H. 2013, MNRAS, 435, 2099
Owen, J. E. 2014, ApJ, 789, 59
Panić, O., van Dishoeck, E. F., Hogerheijde, M. R., et al. 2010, A&A, 519A, 110
Quanz, S. P., Amara, A., Meyer, M. R., et al. 2013a, ApJL, 766, L1
Quanz, S. P., Avenhaus, H., Buenzli, E., et al. 2013b, ApJL, 766, L2
Reggiani, M., Quanz, S. P., Meyer, M. R., et al. 2014, ApJL, 792, L23
Semenov, D., Henning, Th., Helling, M. Ch., & Ilgner, S. E. 2003, A&A, 140, 611
Shakura, N. I., & Sunyaev, R. A. 1973, A&A, 24, 337
Stone, J., & Norman, M. L. 1992, ApJS, 80, 753S
Tatulli, E., Benisty, M., Ménard, F., et al. 2011, A&A, 531, A1
van Leer, B. 1977, JCoPh, 23, 276
Williams, J. P., & Cieza, L. A. 2011, ARA&A, 49, 67
Wolf, S., & D'Angelo, G. 2005, ApJ, 619, 1114
Zhu, Z. 2015, ApJ, 799, 16